Spatiotemporal Electron Beam Focusing through Parallel Interactions with Shaped Optical Fields

F. Javier García de Abajo[1,2,*] and Claus Ropers[3,4]
[1]ICFO-Institut de Ciencies Fotoniques, The Barcelona Institute of Science and Technology, 08860 Castelldefels, Barcelona, Spain
[2]ICREA-Institució Catalana de Recerca i Estudis Avançats, Passeig Lluís Companys 23, 08010 Barcelona, Spain
[3]Department of Ultrafast Dynamics, Max Planck Institute for Multidisciplinary Sciences, 37077 Göttingen, Germany
[4]4th Physical Institute - Solids and Nanostructures, University of Göttingen, 37077 Göttingen, Germany

(Received 31 December 2022; accepted 17 May 2023; published 12 June 2023)

The ability to modulate free electrons with light has emerged as a powerful tool to produce attosecond electron wave packets. However, research has so far aimed at the manipulation of the longitudinal wave function component, while the transverse degrees of freedom have primarily been utilized for spatial rather than temporal shaping. Here, we show that the coherent superposition of parallel light-electron interactions in transversally separate zones allows for a simultaneous spatial and temporal compression of a convergent electron wave function, enabling the formation of sub-Ångström focal spots of attosecond duration. Specifically, spots spanning just ∼3% of the light optical cycle are shown to be formed, accompanied by an increase by only a factor of 2 in spatial extension relative to an unperturbed beam. The proposed approach will facilitate the exploration of previously inaccessible ultrafast atomic-scale phenomena, in particular enabling attosecond scanning transmission electron microscopy.

DOI: 10.1103/PhysRevLett.130.246901

Fourier analysis shows that strongly peaked waveforms can be obtained by superimposing a large number of phase-locked frequency components. This ubiquitous principle underpins pulsed mode-locked lasers and is leveraged to synthesize attosecond light pulses by combining high harmonics generated in atomic gases [1–3] or solid-state targets [4]. Likewise, attosecond electron bunches were formed through interaction with the near fields induced by laser scattering at a periodic structure followed by electron propagation in free space [5], while ponderomotive interaction was predicted to serve the same purpose [6]. In addition, optical near-field interaction and dispersive propagation were predicted to produce attosecond wave packets in the wave function of individual electrons [7], as later demonstrated in experiments using laser scattering by nanostructures [8,9] and also through stimulated Compton scattering in free space [10].

Temporal compression of free-electron beams (e-beams) has a long tradition in the context of accelerator physics and electromagnetic wave generation [5,11–18]. In an intuitive picture, exposure of the e-beam to electromagnetic fields induces a momentum modulation that causes a periodic compression into subcycle bunches upon dispersive propagation of the electron ensemble. By subsequently interacting with gratings [19] or undulators [16], bunches containing a large number of electrons N can produce radiation by acting in unison, giving rise to directed emission with an intensity $\propto N^2$ in what is known as superradiance [20]. This mechanism is widely used in radiation sources operating over spectral ranges extending from microwaves in klystrons [12] to x rays in free-electron lasers [13,14,16,17].

Electron compression can also be accomplished through the coherent evolution of each individual free-electron wave function after interaction with intense optical fields, provided that the level of spatial and temporal coherence of both electrons and light is sufficiently high. For large enough laser intensities, multiple photon exchanges take place, as demonstrated in pioneering experiments of low-energy electron scattering by illuminated atomic targets [21,22]. In the context of ultrafast transmission electron microscopy, this type of process has attracted considerable interest in the form of photon-induced near-field electron microscopy (PINEM) of optical near-field distributions [7,23–29]. In PINEM, electrons emerge in states comprising a superposition of energy sidebands equally spaced by the photon energy. Besides imaging, the quantum-coherent phase modulation underlying the inelastic light-electron scattering process was predicted [7] and experimentally shown [8,9] to produce longitudinal shaping and attosecond bunching. In the momentum representation, the velocity dispersion across the sidebands translates into relative phase differences that accumulate as the probes propagate, developing a periodic train of temporally compressed electron pulses analogous to the Talbot effect [8,30,31].

While a single PINEM interaction is fundamentally limited to produce just a moderate level of temporal compression [32–34], close to perfectly confined pulses are predicted to be formed from a sequence of PINEM interactions separated by free-space propagation [35]. In a

separate development, following the demonstration of ponderomotive phase plates for electron microscopy [36], the possibility of realizing a customizable modulation of the transverse electron wave function profile was proposed using PINEM [37] and ponderomotive [38] light-electron interactions, and recently realized in separate experiments [39,40]. Conceivably, the coherent superposition of electron waves that have undergone distinct PINEM interactions in the transverse plane should grant us access into a much wider range of electron wave functions such as, for example, states that comprise tailored spatiotemporal compression.

In this Letter, we theoretically demonstrate that inelastic electron-light interaction can simultaneously produce spatial and temporal compression. Specifically, we consider a convergent electron wave produced by the objective lens of a scanning transmission electron microscope and study the effect of the interaction with light at a plane preceding the focal plane. For relatively simple transverse field profiles reminiscent of zone plates, we predict the formation of sub-Ångström focal spots of attosecond duration. In particular, a high level of compression is achieved with the superposition of only two wave function components (Fig. 1), while more complex profiles (Figs. 2 and 3) enable a stronger temporal compression without substantially compromising the spatial focusing performance of the microscope. Our work holds potential for the study of ultrafast phenomena at the atomic scale, including highly nonlinear and subcycle charge and lattice dynamics.

Right after interaction with monochromatic light of frequency ω characterized by a space- and time-dependent electric field amplitude $\mathbf{E}(\mathbf{r})e^{-i\omega t} + \text{c.c.}$, the wave function of an electron moving along the z direction with average velocity v becomes [24,41,42]

$$\psi(\mathbf{r},t) = \psi^{\text{inc}}(\mathbf{r},t) \sum_{\ell=-\infty}^{\infty} \alpha_\ell(\mathbf{r}) e^{i\ell\omega(z-vt)/v}, \tag{1}$$

where $\psi^{\text{inc}}(\mathbf{r},t)$ is the incident wave function. The sum in Eq. (1) extends over the net number of exchanged photons ℓ, corresponding to an electron energy change $\ell\hbar\omega$ and having an associated transition amplitude

$$\alpha_\ell(\mathbf{r}) = J_\ell[|\beta(\mathbf{R})|] e^{i\ell \arg\{-\beta(\mathbf{R})\}} e^{-2\pi i \ell^2 z/z_T}, \tag{2}$$

which is expressed in terms of a single electron-light coupling parameter

$$\beta(\mathbf{R}) = \frac{e}{\hbar\omega} \int_{-\infty}^{\infty} dz\, E_z(\mathbf{r}) e^{-i\omega z/v}. \tag{3}$$

We note that Eq. (3) depends on the transverse coordinates $\mathbf{R} = (x, y)$. This result assumes an initial energy spread much smaller than $\hbar\omega$, which is in turn negligible compared with the average kinetic energy (nonrecoil approximation). In addition, a phase $\propto \ell^2$ is incorporated to include the effect of velocity dispersion with a characteristic Talbot distance [30] $z_T = 4\pi m_e v^3 \gamma^3/\hbar\omega^2$, where $\gamma = 1/\sqrt{1 - v^2/c^2}$.

In the spatial representation, the wave function is modulated in time with the optical period $\tau = 2\pi/\omega$ imposed by the light frequency ω. This allows for a quantification of the achieved level of temporal compression through the so-called degree of coherence (DOC) [33,34]. The DOC, defined as

$$\text{DOC}_m(\mathbf{r}) = \left| \int_0^\tau dt |\psi(\mathbf{r},t)|^2 e^{im\omega t} \right|^2 \Big/ \left| \int_0^\tau dt |\psi(\mathbf{r},t)|^2 \right|^2, \tag{4}$$

quantifies the strength of modulation of the electron density throughout an optical cycle. For an index m, it describes to what degree an excitation such as cathodoluminescence generated by the e-beam at position $\mathbf{r}$ and frequency $m\omega$ is coherent with the driving field, a quantity that could be measured from the interference fringes obtained when mixing the emission with a coherent m^{th} harmonic of the driving field. The ideal compression associated with the point-particle limit corresponds to $\text{DOC}_m(\mathbf{r}) = 1$ for all m's.

For a single light-electron interaction, one finds the analytical expression [31,32,34,35] $\text{DOC}_m = J_m^2[4|\beta| \sin(2\pi m z/z_T)]$. For $m = 1$, a moderate maximum value of $\text{DOC}_1 \approx 0.34$ [see Fig. 1(b)] is obtained by adjusting the optical field strength to satisfy the condition $|\beta| = e_1/[4 \sin(2\pi z/z_T)]$, where $e_1 \approx 1.841$ is the argument that maximizes the J_1 Bessel function. As stated above, even tighter compression can be reached by sequential interactions [35]. However, harnessing the transverse degrees of freedom to produce tailored temporal as well as spatial structuring has yet to be explored.

Here, we leverage the coherent superposition of electron wave function components undergoing separate parallel interactions with light in distinct zones for far-reaching spatiotemporal control. Replacing the coefficients in Eq. (2) by a weighted sum with various values of β yields a powerful set of additional control parameters. In a simple picture, temporal compression can be achieved if α_ℓ becomes independent of ℓ over a certain range such as $-L \le \ell \le L$, for which the wave function in Eq. (1) becomes $\psi \propto \sum_{\ell=-L}^{L} e^{i\ell\zeta} = \sin[(L + 1/2)\zeta]/\sin(\zeta/2)$ with $\zeta = \omega(z - vt)/v$, such that $\text{DOC}_m = [1 - |m|/(2L + 1)]^2$ approaches the perfect compression limit for $L \gg 1$. The question we ask is whether ℓ-independent coefficients can be obtained by superimposing parallel electron-light interactions, such that they become

$$\alpha_\ell(\mathbf{r}) = e^{-2\pi i \ell^2 z/z_T} \sum_i a_i J_\ell(2|\beta_i|) e^{i\ell \arg\{-\beta_i\}} \tag{5}$$

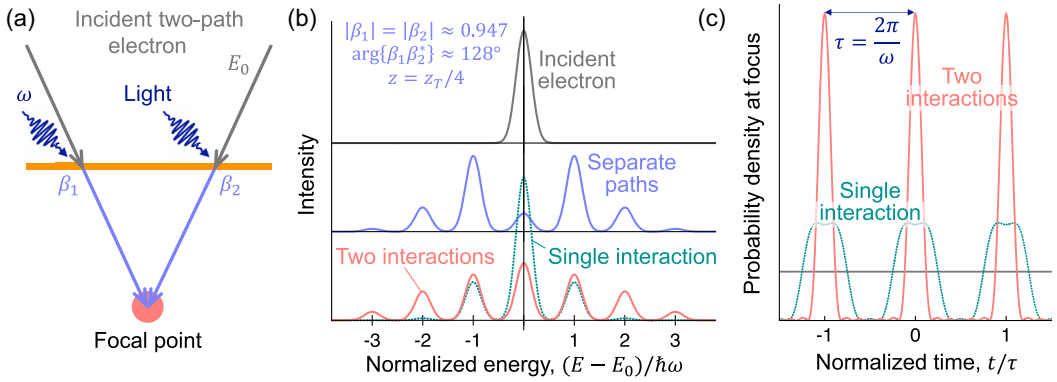

FIG. 1. Temporal compression of a free electron through parallel interactions with optical fields. (a) We consider an incident electron separated into two paths, each of them interacting with light as described by the respective coupling coefficients β_1 and β_2. The two paths are then recombined and brought to interference at a focal point. (b) Spectrum of the incident electron state before (top) and right after (middle) interacting with light, along with the spectrum produced at the focal point by path mixing (bottom). (c) Temporal profile at the focal point, showing a comb of electron probability density with the same period $\tau = 2\pi/\omega$ as the employed light. The interaction coefficients β_i in (b) and (c) are optimized to achieve maximum temporal compression [see β_i values and propagation distance z from optical interaction to focal point in (b)]. We also show results for an optimally compressed single-path–interaction configuration (dotted curves, same z, $\beta = 0.460$).

for a given set of weighting coefficients a_i, with the dispersive phase $-2\pi z/z_T$ proportional to the distance z from a given interaction plane to a common focal spot toward which the electron is converged.

The superposition of wave functions with *two* different electron-light coupling parameters [Fig. 1(a)] is already enough to produce a substantial improvement in temporal compression corresponding to $\mathrm{DOC}_1 \approx 0.84$ [43] and illustrated by the sharp wave function profile plotted in Fig. 1(c), where it is compared with the single-interaction result. The spectral distribution of the wave function resulting from this superposition cannot be achieved with a single interaction [Fig. 1(b)]; it rather approaches a more continuous spectral distribution, as also observed for sequential interactions [35]. This exemplifies a method to produce any designated combination of sideband amplitudes by superimposing a sufficient number of parallel interactions. Incidentally, we impose real coefficients a_i in Fig. 1 (see below), for which the optimum solution involves moderate values of the coupling coefficients β_i [see Fig. 1(b)].

As a practical zone-plate-type configuration, we consider an $\mathbf{R}$-dependent light-electron interaction taking place at a plane situated within the pole piece gap in an electron microscope and before the focal plane, although similar designs could operate by placing the plate at other places along the electron column. Under the paraxial approximation, and assuming axially symmetric coupling coefficients $\beta(\mathbf{R})$ with respect to the e-beam axis at $\mathbf{R} = 0$, the wave function near the focal region is found to take the form of Eq. (1) with coefficients (see details in the Supplemental Material [44])

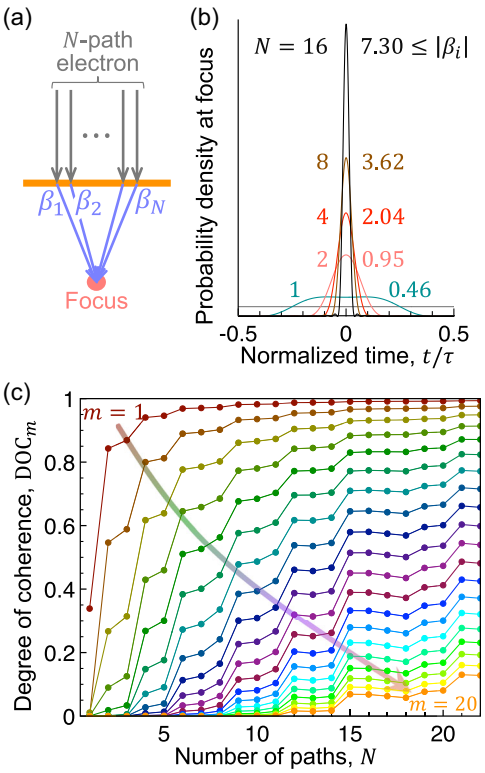

FIG. 2. Optimum temporal electron compression. (a) An increasing number N of parallel interactions with light leads to a narrowing of the probability density peak. The maximum magnitude of the required coupling coefficient is indicated for each considered value of N by color-matching labels. Optimum results are obtained for a propagation distance $z = z_T/4$ in all cases. (b) Degree of coherence DOC_m for optimally compressed electrons after interaction with N parallel zones. We consider harmonic orders $m = 1$–20.

$$\alpha_\ell(\mathbf{r}) \approx e^{-2\pi i \ell^2 z/z_T} \int_0^{\mathrm{NA}} \theta d\theta\, J_0(2\pi\theta R/\lambda_e) e^{-i\pi\theta^2 z/\lambda_e} \times J_\ell[2|\beta(\theta)|] e^{i\ell \arg\{-\beta(\theta)\}}, \quad (6)$$

where NA is the numerical aperture (set to 0.02 in this work), and λ_e is the electron wavelength. This expression is accurate within the paraxial approximation for the wide range of geometrical parameters encountered in currently available electron microscopes (see the Supplemental Material [44]). Incidentally, both spherical and chromatic aberrations can easily be included in our formalism, but are not considered here for simplicity. For concreteness, we consider a stepwise distribution of $\beta(\theta)$ parameters (with the $\mathbf{R}$ dependence now absorbed in the paraxial angle θ; see the Supplemental Material [44]), which could be achieved by projecting a correspondingly shaped laser beam on an electron-transparent film at an oblique angle [46] or, alternatively, by a weakly focused laser beam illuminating a film featuring a stepwise thickness profile consisting of concentric circular (ring-shaped) zones [see Fig. 3(a)]. This configuration reduces Eq. (6) to Eq. (5), with coefficients a_i determined by restricting the θ integral to each of the i zones.

We numerically optimize temporal compression at the focal spot $\mathbf{r} = 0$ (where the coefficients a_i become real) by finding the maximum of $\mathrm{DOC}_1(\mathbf{r} = 0)$ [43] through the steepest-gradient method. Separating the circle defined by the NA in the interaction plane into a total of N equal-area zones [Fig. 2(a)], the coefficients a_i are made independent of i. Under these conditions, the optimum focal electron wave function, represented over an optical period at $\mathbf{r} = 0$ in Fig. 2(b), becomes increasingly sharper as N is increased (see Table S1 in the Supplemental Material [44] for a subset of the obtained optimum values of β_i). Again, realistically attainable values of the coupling coefficients β_i are obtained (i.e., similar to those used in experiments [7,25–27]). Interestingly, optimum results are obtained for a propagation distance $z = z_T/4$ (e.g., $z \approx 2.5$ mm for 60 keV electrons and 4 eV photons), which renders odd ℓ terms in quadrature relative to even terms. The corresponding degree of coherence is calculated analytically for each set of β_i values (see the Supplemental Material [44]) and plotted as a function of the number of zones N and the harmonic order m in Fig. 2(c). A monotonic increase is observed for each order m as N increases, and in particular, we find $\mathrm{DOC}_m > 0.8$ for $|m| \leq 5$ with $N \geq 15$. Although the probability for an electron to undergo inelastic scattering cannot be enhanced by shaping it, as conclusively demonstrated through rigorous theory [42,47], fully coherent excitations can be produced by compressing it when DOC_1 approaches 1 (e.g., a coherent cathodoluminescence emission [33,34]).

The optimum solution at $\mathbf{r} = 0$ is compatible with spatial focusing, as revealed by the analysis presented in Fig. 3. Remarkably, a good level of temporal compression is simultaneously obtained within a finite spatial region covering the focal spot under the configuration presented in Fig. 3(a). At the time of maximum electron density [Fig. 3(b)], the focal spot is laterally confined within a

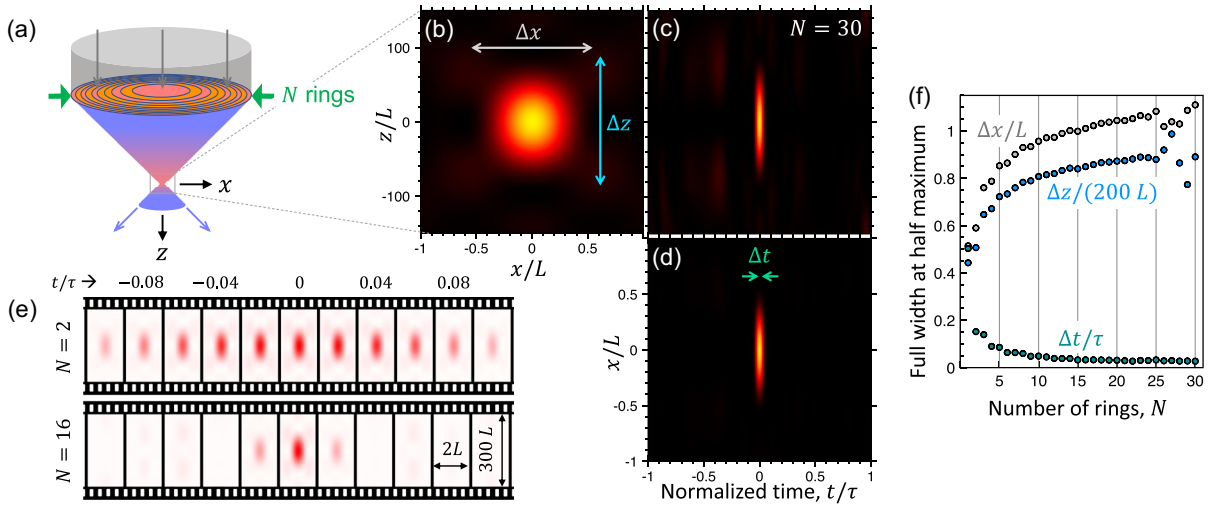

FIG. 3. Focal electron spot profile under temporal compression. (a) We consider a set of N equal-area concentric circular (ring-shaped) zones, each of them delivering a uniform light-electron coupling coefficient. (b)–(d) Upon optimization of the latter for electron temporal compression at the focal spot $\mathbf{r} = 0$ using $N = 30$ zones, we still find a Gaussian-like spatial profile (b) of short duration, as revealed in cuts along both longitudinal (c) and transverse (d) directions. (e) Selection of focal region frames near the time of maximum electron probability reveals a short duration compared with the optical period τ. (f) Width of the focal electron density profile in time (Δt) and along transverse (Δx) and longitudinal (Δz) spatial directions. The pulse duration is shown to decrease with increasing N. All distances are scaled to $L = \lambda_e/\mathrm{NA}$, where λ_e is the de Broglie electron wavelength and NA is the numerical aperture (outer-zone diameter divided by rings-focus distance).

region $R \lesssim \lambda_e/2\mathrm{NA}$ (e.g., ≈1 Å for 100 keV electrons with NA = 0.02) for $N = 30$, whereas it extends over a longitudinal range $|z| \lesssim \lambda_e/(\mathrm{NA})^2$ (≈10 nm). When examining the temporal profile of cross sections passing by the focal spot and oriented along the transverse [Fig. 3(c)] and longitudinal [Fig. 3(d)] directions, we observe an overall level of compression similar to the optimized behavior at the spot center. A similar preservation of spatial focusing is observed with other values of N, while this parameter is primarily affecting temporal compression. For example, the full width at half maximum of the electron density profile is $\approx 0.027\tau$ for $N = 30$, while the spot diameter and longitudinal elongation are roughly a factor of 2 larger than in a temporally unmodulated configuration [see Fig. 3(f)]. For illustration, we present focal spot movies [Fig. 3(e)] revealing the emergence of a sharp electron density distribution within an interval spanning 20% of the optical period for $N = 2$, while shorter focal spot durations are obtained with larger values of N.

In summary, we predict the formation of subnanometer-attosecond spatiotemporal electron probes by molding the transverse electron wave functions through PINEM-like interactions with spatially separated optical fields structured in relatively simple zone profiles. For illumination with 4 eV light, we predict pulses of ∼30 as duration at the expense of a twofold increase in the spatial extension of the focal spot relative to the nonilluminated e-beam. This approach is generally compatible with spatial electron focusing in scanning transmission electron microscopy, where the required optical fields could be directly projected on an electron-transparent plate. Alternatively, a simpler configuration could rely on illumination by a uniform broad light beam, supplemented by lateral structuring of the plate (e.g., a dielectric film coated with metal and forming a layer of laterally varying thickness; see the Supplemental Material [44]). While we have considered monochromatic light, such that a long electron pulse is transformed into a train of attosecond pulses spaced by the optical period, more general illumination conditions relying on broadband fields could be employed to obtain individual electron pulses with much wider temporal separation. As an extrapolation of these ideas, we envision the formation of arbitrary spatiotemporal electron profiles consisting, for instance, of several individual probes at tunable positions and instants to realize subnanometer-attosecond electron-electron pump-probe spectroscopy (e.g., two attosecond electron pulses serving as pump and probe, respectively). A currently attainable light-electron pump-probe scheme could consist in triggering strongly nonlinear processes in a sample through ultrafast laser pulse irradiation, whose fast evolution within a suboptical-cycle timescale could be probed by compressed electrons such as those here investigated.

We thank V. Di Giulio, A. Feist, J. H. Gaida, and S. V. Yalunin for insightful discussions. This work has been supported in part by the European Research Council (Advanced Grant No. 789104-eNANO), the European Commission (Horizon 2020 Grants No. FET-Proactive 101017720-EBEAM and No. FET-Open 964591-SMART-electron), the Spanish MICINN (PID2020–112625 GB-I00 and Severo Ochoa CEX2019-000910-S), the Catalan CERCA Program, and Fundaciós Cellex and Mir-Puig, and the Humboldt Foundation.

*javier.garciadeabajo@nanophotonics.es

[1] P. M. Paul, E. S. Toma, P. Breger, G. Mullot, F. Augé, P. Balcou, H. G. Muller, and P. Agostini, Science **292**, 1689 (2001).
[2] P. B. Corkum and F. Krausz, Nat. Phys. **3**, 381 (2007).
[3] F. Krausz and M. Ivanov, Rev. Mod. Phys. **81**, 163 (2009).
[4] J. Li, J. Lu, A. Chew, S. Han, J. Li, Y. Wu, H. Wang, S. Ghimire, and Z. Chang, Nat. Commun. **11**, 2748 (2020).
[5] C. M. S. Sears, E. Colby, R. J. England, R. Ischebeck, C. McGuinness, J. Nelson, R. Noble, R. H. Siemann, J. Spencer, D. Walz, T. Plettner, and R. L. Byer, Phys. Rev. ST Accel. Beams **11**, 061301 (2008).
[6] P. Baum and A. H. Zewail, Proc. Natl. Acad. Sci. **103**, 16105 (2007).
[7] A. Feist, K. E. Echternkamp, J. Schauss, S. V. Yalunin, S. Schäfer, and C. Ropers, Nature (London) **521**, 200 (2015).
[8] K. E. Priebe, C. Rathje, S. V. Yalunin, T. Hohage, A. Feist, S. Schäfer, and C. Ropers, Nat. Photonics **11**, 793 (2017).
[9] Y. Morimoto and P. Baum, Nat. Phys. **14**, 252 (2018).
[10] M. Kozák, N. Schönenberger, and P. Hommelhoff, Phys. Rev. Lett. **120**, 103203 (2018).
[11] C. M. S. Sears, E. R. Colby, B. M. Cowan, R. H. Siemann, J. E. Spencer, R. L. Byer, and T. Plettner, Phys. Rev. Lett. **95**, 194801 (2005).
[12] A. S. Gilmour, *Klystrons, Traveling Wave Tubes, Magnetrons, Cross-field Amplifiers, and Gyrotrons* (Artech House, Boston/London, 2011).
[13] H. L. Andrews and C. A. Brau, Phys. Rev. ST Accel. Beams **7**, 070701 (2004).
[14] P. Emma *et al.*, Nat. Photonics **4**, 641 (2010).
[15] E. Hemsing, G. Stupakov, D. Xiang, and A. Zholents, Rev. Mod. Phys. **86**, 897 (2014).
[16] C. Pellegrini, A. Marinelli, and S. Reiche, Rev. Mod. Phys. **88**, 015006 (2016).
[17] A. Gover, R. Ianconescu, A. Friedman, C. Emma, N. Sudar, P. Musumeci, and C. Pellegrini, Rev. Mod. Phys. **91**, 035003 (2019).
[18] A. Ryabov, J. W. Thurner, D. Nabben, M. V. Tsarev, and P. Baum, Sci. Adv. **6**, eabb1393 (2020).
[19] S. J. Smith and E. M. Purcell, Phys. Rev. **92**, 1069 (1953).
[20] J. Urata, M. Goldstein, M. F. Kimmitt, A. Naumov, C. Platt, and J. E. Walsh, Phys. Rev. Lett. **80**, 516 (1998).
[21] A. Weingartshofer, J. K. Holmes, G. Caudle, E. M. Clarke, and H. Krüger, Phys. Rev. Lett. **39**, 269 (1977).
[22] A. Weingartshofer, J. K. Holmes, J. Sabbagh, and S. L. Chin, J. Phys. B **16**, 1805 (1983).

[23] B. Barwick, D. J. Flannigan, and A. H. Zewail, Nature (London) **462**, 902 (2009).
[24] F. J. García de Abajo, A. Asenjo-Garcia, and M. Kociak, Nano Lett. **10**, 1859 (2010).
[25] L. Piazza, T. T. A. Lummen, E. Quiñonez, Y. Murooka, B. Reed, B. Barwick, and F. Carbone, Nat. Commun. **6**, 6407 (2015).
[26] O. Kfir, H. Lourenço-Martins, G. Storeck, M. Sivis, T. R. Harvey, T. J. Kippenberg, A. Feist, and C. Ropers, Nature (London) **582**, 46 (2020).
[27] K. Wang, R. Dahan, M. Shentcis, Y. Kauffmann, A. Ben Hayun, O. Reinhardt, S. Tsesses, and I. Kaminer, Nature (London) **582**, 50 (2020).
[28] N. Talebi, Phys. Rev. Lett. **125**, 080401 (2020).
[29] A. Gover and A. Yariv, Phys. Rev. Lett. **124**, 064801 (2020).
[30] V. Di Giulio and F. J. García de Abajo, Optica **7**, 1820 (2020).
[31] M. V. Tsarev, A. Ryabov, and P. Baum, Phys. Rev. Res. **3**, 043033 (2021).
[32] Z. Zhao, X.-Q. Sun, and S. Fan, Phys. Rev. Lett. **126**, 233402 (2021).
[33] O. Kfir, V. Di Giulio, F. J. García de Abajo, and C. Ropers, Sci. Adv. **7**, eabf6380 (2021).
[34] V. Di Giulio, O. Kfir, C. Ropers, and F. J. García de Abajo, ACS Nano **15**, 7290 (2021).
[35] S. V. Yalunin, A. Feist, and C. Ropers, Phys. Rev. Res. **3**, L032036 (2021).
[36] O. Schwartz, J. J. Axelrod, S. L. Campbell, C. Turnbaugh, R. M. Glaeser, and H. Müller, Nat. Methods **16**, 1016 (2019).
[37] A. Konečná and F. J. García de Abajo, Phys. Rev. Lett. **125**, 030801 (2020).
[38] F. J. García de Abajo and A. Konečná, Phys. Rev. Lett. **126**, 123901 (2021).
[39] I. Madan, V. Leccese, A. Mazur, F. Barantani, T. LaGrange, A. Sapozhnik, P. M. Tengdin, S. Gargiulo, E. Rotunno, J.-C. Olaya, I. Kaminer, V. Grillo, F. J. García de Abajo, F. Carbone, and G. M. Vanacore, ACS Photonics **9**, 3215 (2022).
[40] M. C. C. Mihaila, P. Weber, M. Schneller, L. Grandits, S. Nimmrichter, and T. Juffmann, Phys. Rev. X **12**, 031043 (2022).
[41] S. T. Park, M. Lin, and A. H. Zewail, New J. Phys. **12**, 123028 (2010).
[42] F. J. García de Abajo and V. Di Giulio, ACS Photonics **8**, 945 (2021).
[43] The maximum possible value of $\mathrm{DOC}_m = 1$ for any m automatically guarantees $\mathrm{DOC}_m = 1$ for all m's. We therefore maximize DOC_1 with $m = 1$ as a practical procedure to optimize temporal compression. With this goal in mind, we define $\mathrm{DOC}_m(\mathbf{r})$ in Eq. (4) as a quantity normalized to the time-averaged electron probability density at a chosen position $\mathbf{r}$.
[44] See Supplemental Material at http://link.aps.org/supplemental/10.1103/PhysRevLett.130.246901 for further details of the present formalism, where we also include Refs. [30,33,42,45].
[45] M. Abramowitz and I. A. Stegun, *Handbook of Mathematical Functions* (Dover, New York, 1972).
[46] G. M. Vanacore, I. Madan, G. Berruto, K. Wang, E. Pomarico, R. J. Lamb, D. McGrouther, I. Kaminer, B. Barwick, F. J. García de Abajo, and F. Carbone, Nat. Commun. **9**, 2694 (2018).
[47] R. H. Ritchie and A. Howie, Philos. Mag. **36**, 463 (1977).